IEEE Access
The journal for rapid open access publishing

IEEE Xplore Digital Library
http://ieeexplore.ieee.org/Xplore

A Wide-Band Tissue Numerical Model for Deeply Implantable Antennas for RF-Powered Leadless Pacemakers

SAJID M. ASIF[1] *Member, IEEE*, ADNAN IFTIKHAR[2] *MEMBER, IEEE*, BENJAMIN D. BRAATEN [3] *SENIOR MEMBER, IEEE*, DANIEL L. EWERT [3], AND KEITH MAILE[4] *Senior Member, IEEE*

***Abstract*—Radio frequency(RF)-based wireless power transfer (WPT) method is highly desirable to power deep-body medical implants such as cardiac pacemakers. Antenna is one of the essential components of such system, however, it poses significant design challenges for deep-body applications and must be modeled and characterized correctly to achieve the required performance. In this paper, design and validation of a novel wide-band numerical model (WBNM) is proposed for deeply implantable antennas and to enable RF-powered leadless pacing. In particular, we acquired a wide-band tissue simulating liquid (TSL) and fully characterized it using a dielectric probe. Based on the measured properties of the TSL, the design and numerical characterization of the WBNM was performed using a hybrid simulation method, i.e., by employing the finite element method and method of moment. The proposed WBNM was validated experimentally as well as analytically using a reference microstrip antenna. The good agreement between simulated, measured, and analytical results validated the proposed model. Furthermore, the application of this model and the TSL was demonstrated by the design, development, manufacture, and measurement of a novel metamaterial-based conformal antenna at 2.4 GHz. Moreover, good agreement was found between the simulated and measured results of the proposed conformal antenna. It is evident from the results that the proposed numerical model can be used to design deeply implantable antennas for any frequency, ranging from 800 MHz to 5800 MHz. Finally, the proposed miniature conformal antenna and its successful integration with a leadless pacemaker model present a great potential for future RF-powered leadless pacemakers and other deep-body medical implants.**

***Index Terms*—Tissue simulating model, numerical model, leadless pacemakers, implantable antennas, implantable medical devices, energy harvesting, deep-body implants.**

I. INTRODUCTION

WIRELESS powering and recharging of implantable medical devices (IMDs) such as pacemakers is not new [1]–[3], but is lately receiving significant attention [4]–[7]. Research in wireless power transfer (WPT) for biomedical applications, in particular, is considered very important because wireless power is almost a requirement for the IMDs for the reasons of effectiveness, longevity, and more importantly safety. For example, in conventional pacemakers, the transvenous leads and batteries are the biggest problems [8]. The leads may clog the vein and result in pneumothorax, tricuspid valve insufficiency, and infection. Furthermore, the battery has lifetime issues and when depleted, it has to be replaced through a surgical procedure, which is costly and painful for the patient. Moreover, recent statistics have shown that every 14^{th} patient having a pacemaker device in the chest will develop an infection in the pacemaker pocket and among these cases, every 5^{th}, i.e., 20% will result in dealth [9].

To overcome these complications, limitations, and side effects of the conventional pacemakers, researchers have been investigating various modalities to achieve wireless or leadless pacing. Some of the common methods include inductive coupling, magnetic resonance, ultrasonic, radio frequency waves, and even solar power [8], [10]–[12]. Recent developments in the quest for a practical leadless pacemaker include the successful development of Micra TPS (transcatheter pacing system) and Nanostim by Medtronic [13] and St. Jude Medical [14], respectively. However, such devices have a total market of 10-15% because they are single chamber only and hence impractical for multi-site pacing. The need for a similar leadless pacemaker with multi-site pacing capability is critical to address the unmet clinical needs of heart failure patients needing cardiac resynchronization therapy (CRT) [15]. However, the development of such a device is challenging and remains an open problem.

In our previous work [4], we proposed a novel radio frequency(RF)-based leadless pacemaker and demonstrated leadless pacing by performing in vivo experiments using ovine models. The idea reported and demonstrated in [4] is only a proof of concept and hence needs further development as well as improvements toward its practicality. Moreover, the challenging task in the realization of a RF-based wireless system is the design and development of the implantable antenna, which has to be modeled correctly in an environment that correctly emulates the human body [16]. Likewise, the complex lossy nature of the human body and its frequency dependent properties make this task even more challenging. In literature, various tissue simulation models have been proposed [17], [18], but they are either narrow band or frequency specific.

We present a wide-band numerical model (WBNM) using a hybrid simulation technique for time-effective simulations covering the frequency range from 800 MHz to 5800 MHz. In particular, the contributions of this paper are as follows:

1) Design and development of a WBNM and its validation using a reference microstrip patch antenna for the development of deeply implantable antennas.
2) Validation of the proposed numerical model by designing and testing a novel metamaterial-based conformal implantable antenna for leadless pacing.

Digital Object Identifier: 10.1109/ACCESS.2019.2902981

3) Finally, integration of the proposed antenna design with the commercially available leadless pacemaker model to realize and validate the possibility for future RF-powered leadless pacemaker.

In this paper, a full-wave 3D simulation tool, ANSYS High Frequency Structure Simulator (HFSS), was used to design, develop, and validate a WBNM. Employing a reference microstrip patch antenna, the numerical model was validated experimentally as well as analytically. The proposed numerical model was based on a human body tissue simulating liquid (TSL) acquired from SPEAG (Schmid & Partner Engineering AG, Switzerland) [19]. To the best of authors' knowledge, there is no similar wide-band numerical model for the design and optimization of deeply implantable antennas that is reported before. The characterization of the TSL was achieved by measuring its electrical properties using a dielectric probe. The application of this WBNM was also demonstrated by designing a novel conformal antenna at 2.4 GHz. Furthermore, the feasibility of the integration of these proposed antenna with a leadless pacemaker model, similar to Nanostim [14] has been demonstrated. Manufactured on a flexible 10 mil thick Rogers substrate, the implantable antenna prototype was conformed on a 3D printed mock-up leadless pacemaker and measured in TSL. Results of the measurements agree well with the simulations. The compact and cylindrical design of manufactured prototype antenna and its integration with a miniaturized pacemaker model make this method feasible for the leadless pacing applications.

This paper is organized as follows: In Section II, related work on deeply implantable antennas, proposed for wireless powering, is discussed. Relevant details on work related to the dielectric properties and numerical modeling of human body as well as the challenges and limitations of the experimental human body phantoms are also presented in the same section. Section III is dedicated to the investigation of SPEAG's human body tissue simulating liquid and its characterization and results. In Section IV, the design, development, and validation of a wide-band numerical tissue model is discussed by employing a reference microstrip patch antenna. Moreover, the application of the developed numerical model is demonstrated in Section V, which includes the development, manufacturing, and measurements of a deeply implantable conformal antenna for integration with a leadless pacemaker. Finally, discussion is presented in Section VI while the conclusion and proposed future work is summarized in Section VII.

II. Related Work

Every RF-based implantable medical device (IMD) includes at least one implantable antenna, which is usually integrated with additional circuitry whose complexity depends upon the nature of the application of that IMD. Also, every part of a RF-based IMD has its own importance and role in the overall functioning and application, however, the performance of the implantable antenna is critical without which the device may not even function. This highlights the importance of a correct modeling method for the design and development of an implantable antenna, which mainly includes, (a) a human body tissue simulation model, and (b) measurements using an experimental human body phantom.

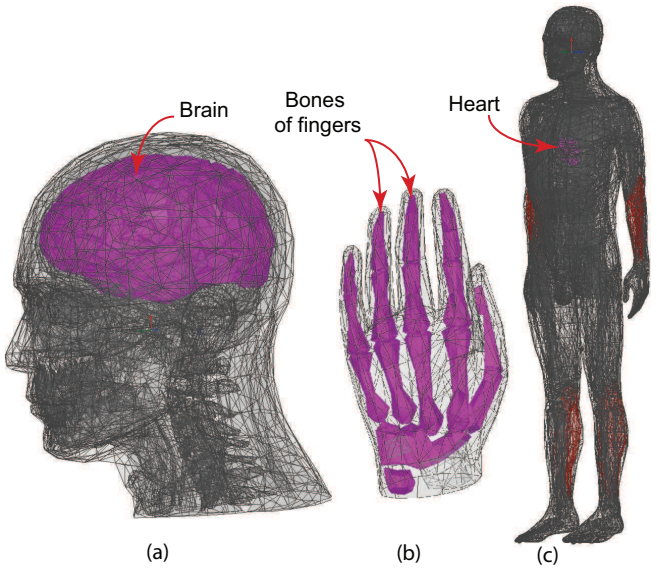

Fig. 1: Different examples of digital human body phantoms, with 2 mm resolution, available in ANSYS HFSS: (a) A human head (brain highlighted), (b) a human left hand (bones highlighted), and (b) a full human body phantom of 35 years old male (heart highlighted).

A. Deeply Implantable Antennas for Wireless Powering

There is a plethora of work reported on wearable and implantable antennas for biomedical telemetry related applications [18], [20] but not much is available on deeply implantable antennas, especially for far-field wireless power transfer (WPT) applications. As mentioned in [21], one of the main obstacles for wireless powering of implantable devices is the attenuation of power density experienced by the propagation of the EM (electromagnetic) waves in the lossy human body. Furthermore, IEEE recommended limits for safe power density and SAR (specific absorption rate) have to be considered for safety, as reported in [21], [22].

Various antennas have been reported for WPT at shallow depths or subcutaneous applications [23]–[26], however, works on implantable antennas for WPT in deep-body tissue applications is very scarce in the literature. Some patents filed in the area of WPT for endoscopic capsules using magnetic coupling of coils are summarized in [27]. Furthermore, a midfield wireless powering method using coils was also proposed for deep-tissue microimplants [28]. A wireless neural recording device using an implantable antenna at a depth of 12 mm inside a phantom has recently been reported in [29]. In [30], a RF-based wireless biomedical system with an on-chip antenna and CMOS diodes are proposed for Glaucoma intraocular and cardiovascular pressure monitoring. In [4], a planar rectenna-based leadless pacemaker was demonstrated in ovine models at 1.2 GHz. Literature survey on WPT revealed that previous work has been progressive, however, the practicability of miniaturized and conformal deeply implantable antennas on

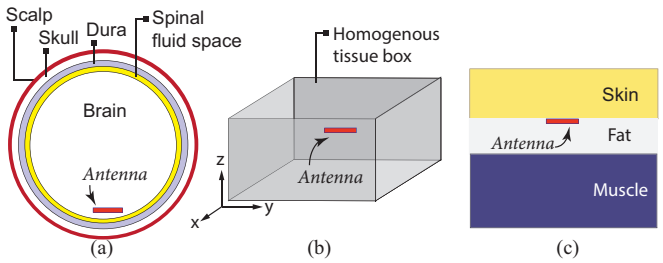

Fig. 2: Various examples of phantom geometries used in numerical methods for the design and development of implantable antennas. (a) A spherical multi-layer head model, (b) a muscle equivalent phantom, and (c) a 3-layer model representing skin, fat, and muscle of the human body.

commercially available pacemakers has not been addressed in the literature.

B. Dielectric Properties and Numerical Modeling of the Human Body

A summary of literature on the dielectric properties and various methods of human body tissue modeling is described in [31], [32]. Implanted antennas are completely embedded inside the human body, which consists of time-varying lossy dielectric materials (including skin, fat and muscle etc.). It is hence critical that besides the modeling and optimization of the antennas, special consideration has to be given to the human body modeling in the available simulation tools. Some advanced 3D EM solvers for the design and development of implantable antennas and other RF based-biomedical devices and systems include: (1) ANSYS High Frequency Structure Simulator (HFSS), which is based on the finite element method (FEM) [33]; (2) Computer Simulation Technology (CST) Studio Suite, which provides access to multiple electromagnetic (EM) simulation solvers which use methods such as the finite element method (FEM) the finite integration technique (FIT), and the transmission line matrix method (TLM) [34]; and (3) ZWT-SPEAG's Sim4Life, which uses finite-difference time-domain (FDTD) method [35].

Based on the capabilities of CST and HFSS, researchers have been designing their own anatomical numerical models of human body tissues and have also employed digital human body phantoms readily available in these tools [17], [36]. It is noted that the selection of these tools has mostly been dependent upon the availability and personal preference rather than the performance, as both have similar characteristics. Nevertheless, the computational cost (processing power of the machine and the time etc.) is all dependent upon the model and structure of the antenna and also on the complexity of the tissue.

There are various ways in which these numerical simulations can be employed for the design of the implantable antennas. Anatomical human tissue models may provide better and more realistic results but the associated cost and the computational time is higher. Examples of some digital phantoms with high resolution of the human body in HFSS is shown in Fig. 1. Different geometries, uniform and nonuniform models can be designed with a single or multilayer configurations, as presented in the examples illustrated in Fig. 2. In [17], it is shown that similar results can be achieved while using a multilayer canonical model as compared to a realistic human chest model. Also, the performance of another implantable patch antenna, designed in [16], showed similar agreement when results of using a three-layer spherical model were compared against the study repeated using an anatomical model of the human head.

The multilayer canonical models are proven to provide an acceptable model for the human body. When considering a detailed design modeling of the human body, each biological tissue is assigned specific properties including the relative permittivity ε_r, conductivity σ and mass density ρ values. These properties (ε_r, σ) are frequency dependent, the frequency dependency of which is taken into consideration by employing various algorithms based on the Cole-Cole models [37] or Debye models [38]. An extensive detail of the dielectric properties of the human body tissues at a range of radio frequency and microwave frequencies is available in the literature [39], [40].

C. Challenges and Limitations of Experimental Human Body Phantoms

Following the design, optimization, and fabrication of an implantable antenna, correct measurements of its performance parameters are very important. The performance of implantable antennas can be measured in various kinds of phantoms, which emulates the correct dielectric properties of the human body. These phantoms provide a practical platform for testing of the implantable antennas and the process depends on the type of phantom being used. A fabricated prototype is either fully immersed, inserted or carefully placed inside the phantom and then results are taken using a calibrated network analyzer. To fully validate a model, it is recommended to create an identical scenario to the one used in the numerical tool and also consider the overall application.

The main challenge with these phantoms is the overall formulation. The final phantom should be free of any air bubbles and also during preparation, the mixture has to be carefully stirred while being heated and also, the ingredients have to be added at certain temperatures during the process. Furthermore, most of these phantoms are very narrow band and a little imperfection in the preparation process can be unfavorable.

The ingredients of the phantom recipes mainly include DI (Deionized) water, salt, sugar, gelatine, soap, and oil. It is shown that increasing the sugar concentration decreases ε_r, while also contributes towards a slight decrease in σ. Also, adding more salt to the solution causes a significant increase in σ, while the ε_r decreases [37]. Overall, the available phantoms can be categorized into three types, i.e., liquid, semisolid, and solid phantoms [41].

Liquid phantoms are easy to prepare and, depending on applications, can be contained in a variety of container shapes. However, these phantoms have to be carefully selected as they

can often influence the overall properties. Liquid phantoms have relatively shorter shelf life and in addition, only cover frequency up to 6 GHz [19], [16]. Whereas, solid phantoms (gel phantoms) can be used to manufacture a layered heterogeneous phantom and are preferred for their long-term stability and ease of use. Gel phantoms have been proposed for frequency range from 500 MHz to 20 GHz [42], [44], [45], [53]. On the other hand, solid phantoms as compared to semi-solid phantoms (liquid and gel phantoms) have a longer shelf life, but are available up to 6 GHz. Moreover, these phantoms are very expensive to manufacture and require complex manufacturing processes [46]–[48].

A brief overview on the available simulation models acquired from the experimental human body phantoms demonstrated that no standard procedure has been adopted to numerically validate a deeply implantable antenna in human body tissues' numerical model. Moreoever, complete human body phantoms available in 3D EM solvers add huge computational complexities and require a relatively large simulation time. Therefore, a procedure of validation and development of a wide-band simulation model, to emulate the human body tissue, can provide flexibility and adaptability to the designer to work efficiently and progressively in designing deeply implantable antennas, while reducing the computational complexities using the proposed hybrid simulation technique in HFSS.

III. SPEAG'S HUMAN BODY TISSUE SIMULATING LIQUID (TSL)

In order to design, develop, and optimize a human body tissue simulating liquid (TSL) in a numerical tool, such as HFSS, a commercially available wide-band tissue simulating model (phantom), acquired from SPEAG (Schmid & Partner Engineering AG, Switzerland) [49] was selected in this work. The rationale behind this choice was to select a standard TSL, and also to minimize the limitations and complexities of the available phantoms, as mentioned in the previous section.

The category of simulating liquid acquired for this work was human body TSL and its product and batch numbers were 'SM AAM U16 BD' and '160218-1', respectively. The recommended frequency range for this specific TSL was from 800 MHz - 5800 MHz. It is worth mentioning that SPEAG's TSL is mainly used for SAR (specific absorption rate) measurements in MRI (magnetic resonance imaging) applications and that the authors could not find its use for implantable antennas in the available literature. The numerical model of a wide-band tissue simulating liquid is the first proposed model reported on a standard commercially available TSL.

A. Characterization of Body Tissue Simulating Liquid (TSL)

SPEAG, the manufacturer of TSL, provided the dielectric properties of the given TSL, which were measured using a DAK 3.5 dielectric kit [50]. However, to propose a numerical model, the dielectric properties of TSL were first validated using a calibrated Keysight's N1501A Dielectric Probe Kit and then compared with the TSL data sheet [49]. The dielectric properties included relative permittivity-real ε_r', relative

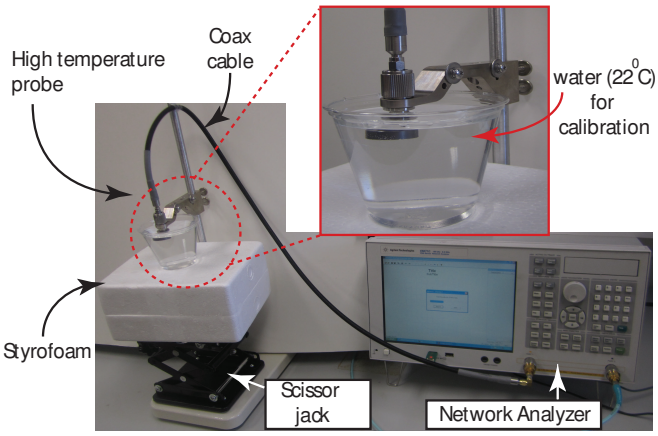

Fig. 3: A picture of the complete calibration setup of the Keysight N1501A, high temperature dielectric probe kit (inset shows the probe inserted in water at 22 °C).

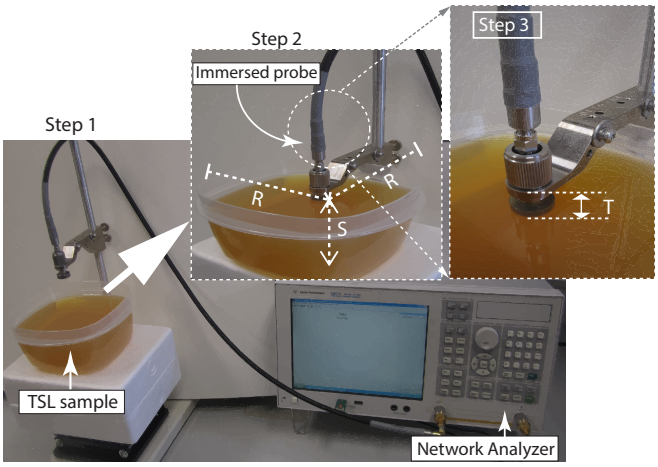

Fig. 4: A picture of the experiment setup used for measuring the dielectric properties of the SPEAG's human body tissue simulating liquid (TSL). Dimensions are in cm: $R = 15$, $S = 6.5$ and $T = 1.2$.

permittivity-complex ε_r'', conductivity σ and loss tangent $\tan\delta$. The N1500A materials measurement suite was first installed on the E5071C vector network analyzer (VNA) and then the high temperature probe was connected to the VNA using a coaxial probe to perform the measurements. It is important to note that prior to perform any measurements, the VNA as well as the dielectric probe was fully calibrated. Deionized water was used for calibration, as shown in the calibration setup in Fig. 3. The actual measurement procedure is summarized as follows: (a) Select the range of frequencies and the type of sweep that you want to perform. (b) Calibrate the entire system by using three known standards, i.e., air, a short circuit, and water (deionized). (c) Insert the probe into a sample of the TSL and take the required measurements. In this work, each property (ε_r, σ, etc.) is measured separately and one at a time.

Following the calibration procedure, the measurement setup, specifically the coaxial cable and the high temperature probe, should not be moved or else calibration may get affected.

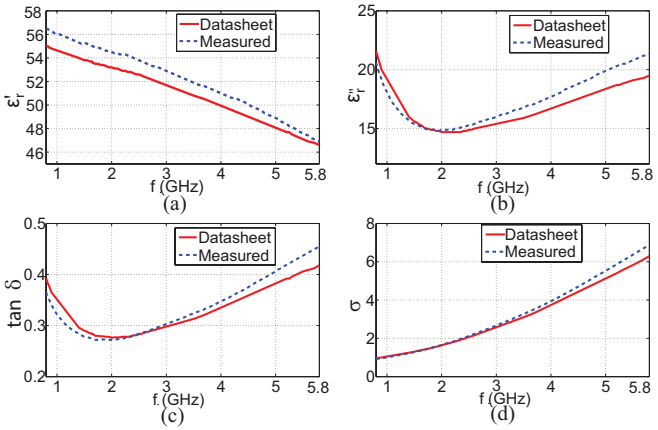

Fig. 5: Comparison of the measured properties of SPEAG's TSL with the data sheet. (a) Real part of the relative permittivity ε_r', (b) complex part of the relative permittivity ε_r'', (c) loss tangent $\tan\delta$, and (d) conductivity σ.

In this method, a metallic scissor jack was used to support the container (containing the sample of TSL) which provided additional stability to the measurement setup. To minimize the effect of the metallic scissor jack on the actual measurements, a 10 cm thick Styrofoam block ($\varepsilon_r = 1.03$) was inserted between the scissor jack and the measuring sample. The properties of the SPEAG's human body TSL were measured using the above stated method and the experiment setup is shown in Fig. 4.

The quantities directly measured by the calibrated dielectric probe were, (a) real part of the relative permittivity ε_r', (b) complex part of the relative permittivity ε_r'', (c) loss tangent $\tan\delta$, and (d) Cole-Cole diagram. The conductivity (S/m) of the TSL however, was computed using the following expression:

$$\sigma = 2\pi f \varepsilon_r'' \varepsilon_o \quad (S/m), \tag{1}$$

where f is the frequency in Hz, ε_r'' is the complex permittivity measured by the probe at a specific frequency f and ε_o is the free space permittivity ($\varepsilon_o = 8.85412 \times 10^{-12} F/m$).

B. Comparison of Measured Dielectric Properties with Data Sheet

The measured dielectric properties of the TSL were compared with the values provided in the data sheet and showed good agreement, as shown in Fig. 5. The agreement between the data sheet and measured values of the TSL properties confirmed the validity of the reported properties of the TSL. This further validates the SPEAG's TSL phantom suitability for implantable antenna measurements for a range of frequencies, i.e., 800 MHz to 5800 MHz.

IV. Design, Development, and Characterization of the Numerical Model

ANSYS's High Frequency Structure Simulator (HFSS), version 17.1, was used to design and develop the numerical model for the implantable antennas. A step-by-step procedure with a brief description of each process is presented in Fig. 6. In the first phase, specific geometry of the model was designed after the selection of phantom type discussed in Section II. Then, the designed model was assigned measured frequency dependent properties using Cole-Cole models or Debye models. In the second phase, the designed geometry with the assigned frequency dependent properties was validated and compared with the measured dielectric properties of the commercially available phantom type, i.e., tissue simulating liquid. Once the numerical model was validated, a reference antenna was designed in the numerical model and simulation results were analyzed. In the third phase, antenna was fabricated and tested in the TSL which was mimicked in the simulations. In parallel, same reference antenna's characteristics were computed analytically using design equations. Following the agreement of the simulated, measured, and analytical results, the numerical model was declared validated.

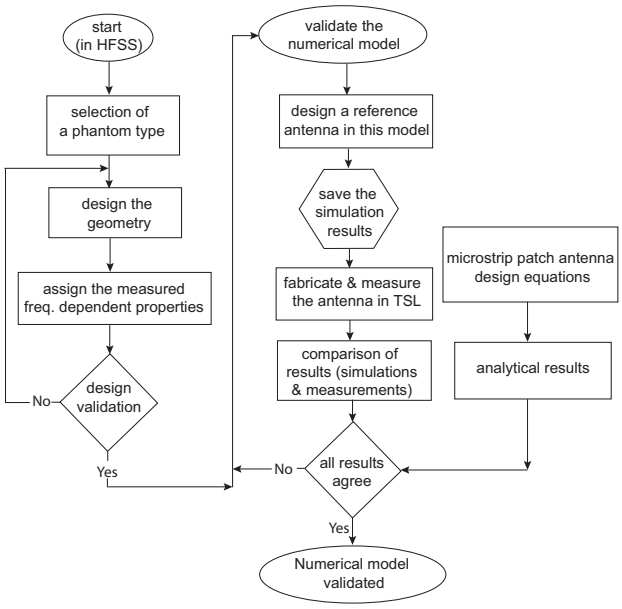

Fig. 6: A flowchart showing important steps performed in the design, development, and validation of the numerical model for deeply implantable antennas.

With regards to the selection of the phantom type in HFSS, we created an exact replica of the experiment setup designed and manufactured for the measurement of the implantable antenna prototype. This consisted of a cubical Plexiglas container measuring approximately 30 cm on each side and filled with SPEAG's TSL (up to 8.0 cm $\approx$ 7.0 liters). The dielectric properties, i.e., the relative permittivity ε_r and conductivity σ assigned to the Plexiglas container were 3.4 and 0, respectively. For the TSL however, the measured frequency dependent properties (from 800 MHz - 5800 MHz) were assigned. To satisfy the boundary conditions in HFSS, this setup was enclosed in a radiation box, which was kept at a distance of $\lambda_o/4$ away from the structure (λ_o being the free space wavelength). A 3D sketch of this model is shown in Fig. 7.

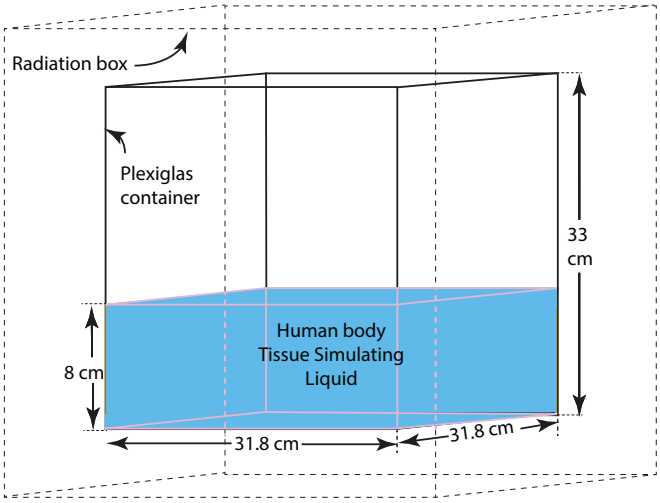

Fig. 7: An illustration of the geometry (with complete dimensions) of the experimental setup of the TSL modeled in HFSS.

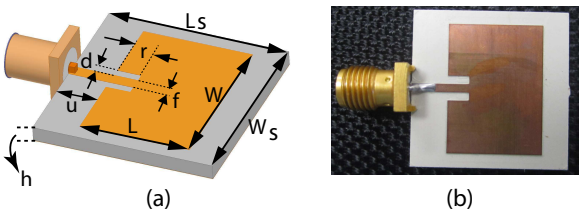

Fig. 8: A 5.0 GHz reference microstrip patch antenna. (a) a 3D antenna model (Dimensions are as follows (all in mm): L=13.38, W = 18.24, L_s=W_s = 22, h = 1.52, d = 1.3, f = 1.4, r = 4, u=5), and (b) a picture of the manufactured prototype reference patch antenna.

A. Designing a Reference Microstrip Patch Antenna

In order to fully validate the proposed model developed for the implantable antennas, it was important to complete the characterization and testing of the proposed model using a reference antenna. Therefore, a reference microstrip patch antenna was designed in HFSS for air. A patch antenna was selected because its a low profile antenna, easy and inexpensive to manufacture, and more importantly can be validated using the equations given in [51]. Reviewing the range of the frequency dependent properties of the given TSL, 5.0 GHz was selected as the resonant frequency for the design of this reference patch antenna (RPA). The aim was to design a microstrip RPA that would resonate at a higher frequency in air or free space, and then model and measure the same prototype in the TSL to observe a frequency shift. It was therefore envisioned that for the same reference antenna, when tested in SPEAG's human body TSL (being a lossy medium), a lower resonant frequency would be achieved.

B. Prototype Fabrication and Measurements in Air

A patch antenna with an inset microstrip feed line (matched to 50 Ω) was designed, simulated, and optimized using a full-wave 3D electromagnetic solver, ANSYS HFSS. This

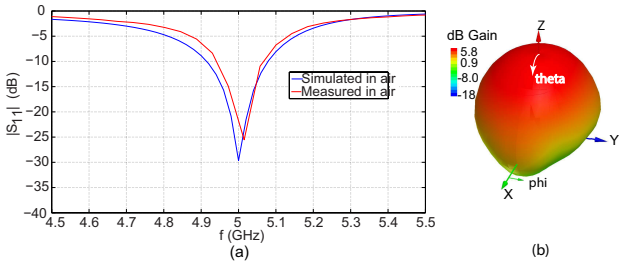

Fig. 9: Performance of the reference patch antenna: (a) Comparison of the simulated and measured reflection coefficients ($|S_{11}|$ in dB), and (b) a simulated 3D radiation plot showing total gain (in dB).

antenna was designed and fabricated on a 1.52 mm thick Rogers TMM4 substrate, having a relative permittivity ε_r of 4.5, loss tangent $\tan\delta$ of 0.002, and copper lamination thickness of 17.5 μm. A complete 3D model with details of the geometry and a picture of the antenna prototype are shown in Fig. 8 (a) and (b). Following the fabrication of the antenna, the whole prototype was insulated with a thin layer (approximately 0.01 μm) of conformal coating. The antenna was insulated because eventually it had to be tested in the TSL (which is conductive) and effects on the resonant frequency in both cases, air and the TSL were of interest.

The reflection coefficients ($|S_{11}|$ in dB) of the manufactured prototype antenna were measured in a calibrated anechoic chamber and results were compared with the simulation. Fig. 9 (a) shows good agreement between the simulated and measured results. The simulated 3D radiation plot showing a total gain of 5.8 dB is shown in Fig. 9 (b).

C. Hybrid Numerical Modeling Method in HFSS

Following the successful design and measurement of the RPA in air, the same antenna (without any modification) was inserted, as a 3D component, into the TSL inside the Plexiglas container in the numerical model created in HFSS, as shown in Fig. 7. Because of the larger electrical size of the setup and to save both the computational time and cost, an integral equation solver (Domain Decomposition) in a hybrid simulation type was employed for this complex case.

Specifically, the configuration of hybrid simulation was performed as follows: First, the RPA was enclosed in a small box, measuring 8 mm × 14 mm × 20 mm, and was assigned the measured frequency dependent properties of the TSL. The walls of this box were kept $\lambda_{TSL}/10$ away from each corner of the antenna model (λ_{TSL} being the wavelength in TSL). This small box was then subtracted from the TSL (filled in the Plexiglas), with a clone object tool selected. The TSL outside the small box was then defined as a dielectric cavity. This process essentially divided the whole TSL into two regions, one with the antenna enclosed in a smaller box and the second with the TSL outside the small box. The main reason for this segregation was to enable HFSS to solve the antenna including the smaller box using the finite element

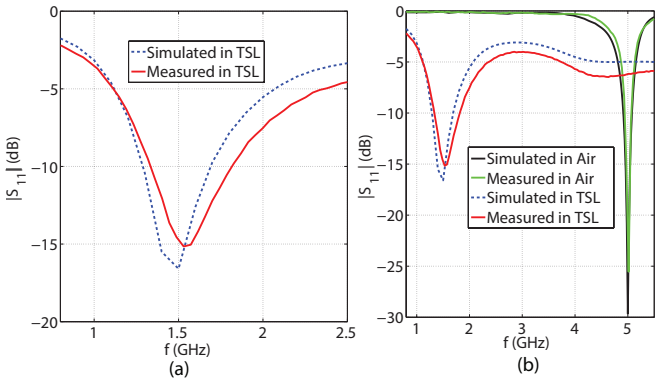

Fig. 10: Comparison of the simulated and measured results. (a) Comparison of measured and simulated $|S_{11}|$ in TSL, (b) Comparison of results taken in air and TSL showing frequency shift.

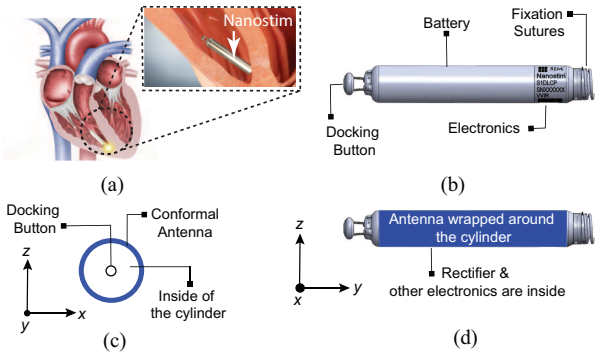

Fig. 11: (a) St. Jude's Nanostim leadless pacemaker (NLP) positioned in the right ventricle (RV). (b) Details of the various components of the NLP. (c) Proposed modifications to the NLP showing two different orientations of the conformal antenna wrapped around the circumference of the NLP.

method (FEM) and the remaining geometry (including the TSL) using the method of moment (MoM). This process enabled the efficient use of resources and saved simulation time significantly. All the simulations were performed under a high performance computing (HPC) license on a powerful machine, having two processors (Intel Xeon(R) CPU E5-2699 v3 2.30 GHz) with 16 cores each and 192 GB of dedicated RAM.

D. Comparison and Validation of the Results in Tissue Simulating Liquid

Results obtained from the HFSS simulations were then compared with the measurements performed in the TSL. As shown in Fig. 10, results agreed well with each other and as expected, the resonant frequency of the RPA got shifted from 5.0 GHz, in air, to a lower resonance, i.e., 1.5 GHz when inserted in TSL. This was further validated using the equations given in [52].

The wavelength in air for the given case is computed as,

$$\lambda_{air} = \frac{c}{f\sqrt{\epsilon_r}}. \tag{2}$$

Then, by using the given values, the guided wavelength of RPA in air is,

$$\lambda_{air} = 28.28\ mm. \tag{3}$$

The actual radiating length (L) of the RPA is 13.38 mm, hence the electrical length of the RPA w.r.t. the guided wavelength can be computed as,

$$L_{air} = 0.473\,\lambda_{air} \approx 0.5\,\lambda_{air}. \tag{4}$$

Similarly, the above steps are repeated for the RPA when radiating in the TSL. It is observed the resonant frequency of the RPA in TSL is 1.56 GHz, and the measured relative permittivity ϵ_r of the TSL at 1.56 GHz is 55.2 and relative permittivity of RPA substrate is 4.5. The guided wavelength of the RPA in TSL with $\epsilon_{rTSL} = 59.7$ is hence given by,

$$\lambda_{TSL} = \frac{c}{f\sqrt{\epsilon_{rTSL}}}. \tag{5}$$

Then by using the given values, the wavelength in the TSL is,

$$\lambda_{TSL} = 24.88\,mm. \tag{6}$$

The actual radiating length (L) of the RPA is 13.38 mm, hence the electrical length of the RPA w.r.t. the wavelength in TSL can be computed as;

$$L_{TSL} = 0.53\,\lambda_{TSL} \approx 0.50\,\lambda_{TSL}. \tag{7}$$

This implies that,

$$L = L_{air} = L_{TSL} = 0.50\,\lambda_{air} = 0.50\,\lambda_{TSL}. \tag{8}$$

It is hence shown that the resonant frequency of this RPA is the function of its length, which is consistent both in air, and also in the tissue simulating liquid. Moreover, for the given relative permittivity ϵ_r of 4.5 and resonant frequency of 5.0 GHz, the length L and width W of the RPA, computed using the microstrip patch antenna equations [52], resulted in the dimensions of 13.64 mm and 18.08 mm, respectively. Compared to the measured values (L & W) of 13.38 mm and 18.24 mm, the percentage error was found to be 1.9 % and 0.9 %, respectively. This further validates the accuracy of the numerical model created in HFSS, for the design and optimization of the implantable antennas.

V. Applications of the Developed Numerical Model

Following the characterisation and validation of the proposed numerical model for deeply implantable antennas, we employ the developed numerical model for the development of an antenna for practical application, i.e, a RF-powered leadless pacemaker.

A. Design Concept of a Novel Leadless Pacemaker

As mentioned in Section I, the main goal of developing a wide-band numerical model was to provide a platform for the design and development of deeply implantable antennas, especially for leadless pacing. To devise a more practical

leadless system, a novel metamaterial-based conformal implantable antenna for integration with a pacemaker design, similar to Nanostim [14], is proposed. The design concept of this system is illustrated in Fig. 11(a)-(d).

It is also envisioned that the integration of a conformal implantable antenna with the commercially available casing of a device similar to Nanostim, as shown in Fig. 11 (b), will be a more practical and realizable solution for leadless pacing. The conformal antenna wrapped around the cylindrical pacemaker will receive the power from the incoming RF waves (transmitted from outside to inside the body) and then provide this power to the circuitry enclosed inside the cylinder (device) for energy harvesting and eventually pacing the myocardium. With no battery requirements, this proposed leadless pacemaker model can be a good candidate for future RF harvesting leadless pacing applications.

B. A complimentary split-ring resonator (CSRR)−loaded deeply implantable conformal antenna

To achieve a novel deeply implantable conformal antenna for leadless pacing, a resonant type metamaterial technique, i.e., a complimentary split-ring resonator (CSRR) has been used in this work. This technique provided the flexibility to achieve the required resonance frequency, and also helped in achieving a compact design with relatively good performance. The resonance frequency for this antenna was decided to be 2.45 GHz, which is an available open band in the industrial, scientific and medical (ISM) radio bands.

The proposed numerical model, developed in Section IV-A, was employed for the design and development of this conformal deeply implantable antenna. A 10 mil thick Rogers 6010LM substrate, having a dielectric constant ϵ_r of 10.2 was selected for this application. This substrate was selected due to its flexibility and high dielectric constant, which helped in achieving a conformal and compact design. A dummy cylindrical pacemaker measuring 20 mm in length and 6 mm in diameter was first created in HFSS and then the implantable antenna was conformed around this cylinder. With 17.5 μm of copper thickness on each side of the substrate, the overall thickness of the antenna was 0.289 mm. When the antenna was wrapped around the circumference of the cylinder, the total diameter of this model increased to 6.578 mm. A detailed geometry with dimensions of the implantable antenna and the dummy pacemaker is shown in Fig. 12 (a-c).

The dummy cylindrical shaped pacemaker was designed in Solidworks, and manufactured using a desktop 3D printer (MakerBot Replicator). Also, the antenna was fabricated using the LPKF S63 Protomat milling machine and then tightly wrapped around the 3D printed pacemaker model using a clear adhesive. A 50 Ω SMA connector was connected to the conformal antenna prototype for testing purposes, as shown in Fig. 12(d). The manufactured prototype was conformal coated for insulation purposes before immersing it 5 cm deep inside the tissue simulating liquid for performance measurements. This measurement setup, showing a Keysight E5071 network analyzer and a Plexiglas container filled with TSL is shown in Fig. 13. A comparison of simulated and measured matching

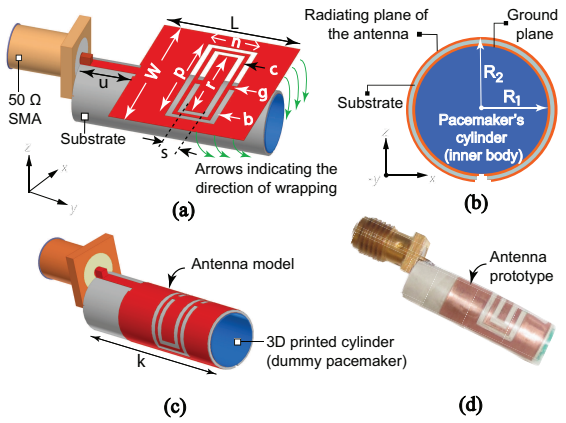

Fig. 12: (a) The geometry details of the CSRR unit cell. (b) A 3D model of the CSRR loaded conformal antenna with complete model of the pacemaker (dummy). (c) A picture of the manufactured prototype. All dimensions are in mm: $u = 5.7$, $L = 14.28$, $W = 17.28$, $p = 14$, $r = 10.8$, $g = 0.75$, $s = 2.0$, $n = 5.2$, $k = 20$, $d = 6.5$, $c = 0.4$, $b = 0.6$, $R_1 = 6.0$, and $R_2 = 6.578$.

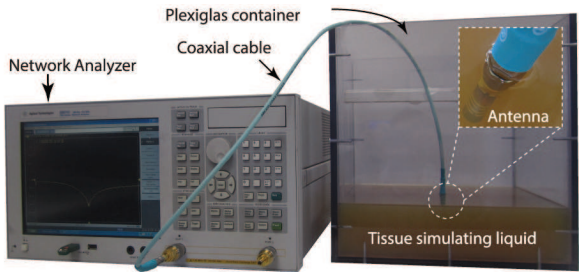

Fig. 13: A picture of the experiment setup showing CSRR-loaded conformal antenna being measured in the TSL.

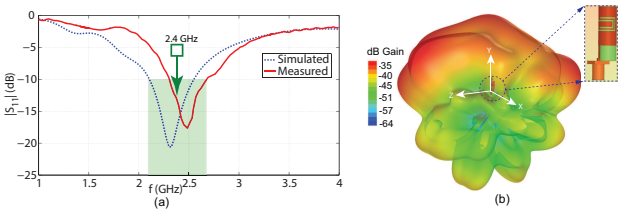

Fig. 14: Performance of the CSRR loaded conformal antenna. (a) Comparison of the simulated and measured reflection coefficients ($|S_{11}|$ in dB). (b) A 3D plot showing the total gain.

performance has shown a good agreement, as shown in Fig. 14. The measured 10 dB return loss bandwidth was found be approximately 300 MHz. Although the measurements were performed in a fully calibrated anechoic chamber, a small frequency shift in the measurements was observed, which was attributed to the fabrication and manufacturing imperfections of the prototype.

VI. Discussion

In literature, researchers have been using cube or cylindrical layered model for emulating human body tissues, as summarized in Section II. However, the previously reported models are narrow band and designers face computational complexities while designing deeply implantable antennas. Therefore, the main emphasis of this work is on the development and validation of a wide-band tissue numerical model for deeply implantable antennas. A microstrip patch antenna owing to its simple structure and shape flexibility attribute was selected to validate the proposed WBNM. However, this platform can certainly be used for other biomedical applications involving the design of deeply implantable antennas. For designing an implantable antenna for a tissue, the designer would first need to validate a numerical model using the flowchart shown in Fig. 6 having dielectric properties of that specific tissue where the implant would reside. Also, using this developed wide band model and proposed hybrid technique discussed in Section IV, designer can easily simulate and validate deeply implantable antennas for the future wireless pacing or similar applications.

Following the validation of the numerical model, a conformal antenna integrated with a dummy pacemaker further emphasized the realizability of the proposed wide band numerical method and its applicability in designing leadless pacemakers. The design concept of the proposed system was adapted from Nanostim and was favored due to its less invasive delivery method using femoral artery. It is important to note that the overall size of our proposed leadless pacemaker, with the conformal antenna included, is smaller than Nanostim, i.e, a total volume of $0.68\,cm^3$ compared to $1\,cm^3$.

Furthermore, the numerical model was proposed to mimic human body tissue for cardiac implantation. The proposed numerical model has a limitation as it cannot be used to model and characterize antennas implanted close to the boundaries between two tissues because of different dielectric properties of the tissues. On the other hand, for a deeply implantable antenna in a tissue, the far-field region of the antenna would be much less as compared to free space far-field [52] because of lossy nature [39] of the human tissue. Thus, surrounding tissues would not effect the characteristics of the implant antenna and proposed numerical model can be employed to design deeply implantable antennas in tissue.

The long term goal of this study is to develop a multi-site and leadless pacing system, which will be capable of addressing the unmet clinical needs of the CRT patients. One potential method of achieving leadless CRT, using six leadless pacemakers implanted at the (1) right atrium, (2) left atrium, (3) right ventricle, (4) left ventricle, (5) right ventricle apex, and (6) left ventricle apex, of a human heart model is shown in Fig. 15 (a). Furthermore, a wearable transmitter with a conformal transmitting antenna array is depicted in Fig. 15 (b). The developed numerical model and the proposed hybrid simulation technique can be used to develop six leadless pacemakers in heart and then designing a wearable transmit array on the skin tissue for wireless power transfer applications.

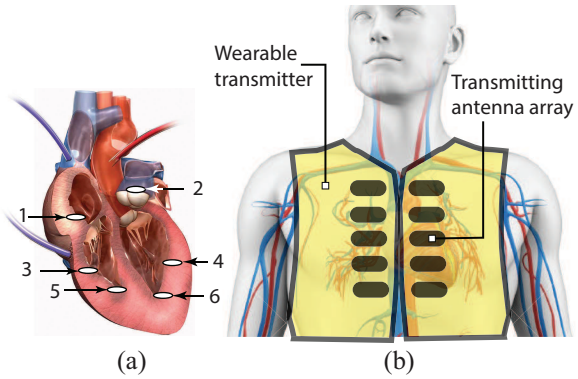

Fig. 15: An conceptual illustration envisioning the implantation of (a) multiple leadless pacemakers at (1) right atrium, (2) left atrium, (3) right ventricle, (4) left ventricle, (5) right ventricle apex, and (6) left ventricle apex, and (b) a wearable transmitter with a conformal transmitting antenna array.

VII. Conclusions

In this paper, a novel wide-band tissue simulation model has been designed and developed for deeply implantable antennas. More specifically, it is shown that a commercially available tissue simulating liquid (TSL) can be used to design a wide-band numerical model. This model was further validated experimentally and analytically using a reference microstrip patch antenna. The application of this numerical model was demonstrated by the design and development of a metamaterial-based deeply implantable conformal antenna. Furthermore, integration of the proposed antenna with a model of a leadless pacemaker was presented as a solution to tackle the multi-site pacing needs for patients requiring CRT. Moreover, it was shown that adopted hybrid technique in the proposed numerical model can reduce computational cost as compared to the human phantoms. Overall, the simulated and measured results of the characterization of TSL, reference microstrip patch antenna, and the proposed conformal antenna, were found to be in good agreement with each other. Overall, the validation procedure of WBNM proposed in this work has a great potential to help designers in modeling any human tissue model for deeply implanatable biomedical sensors and antennas.

Acknowledgment

The authors would like to recognize the technical staff at Boston Scientific, Arden Hills, MN, for their excellent support during this project. S. M. Asif completed this work as part of his Ph.D. degree at the North Dakota State University, USA.

References

[1] W. D. Widmann, *et al.*, "Radio-Frequency Cardiac Pacemaker," *Ann. N. Y. Acad. Sci.,* 1964, pp. 992–1006.

[2] C. Cammilli, *et al.*, "Radio-Frequency Pacemaker with Receiver Coil Implanted on the Heart," *Ann. N. Y. Acad. Sci.,* 1964, vol. 111, 1749 - 6632.

[3] R. Bashirullah, "Wireless implants," *IEEE Microwave Mag.,* vol. 11, no. 7, pp. 114 - 123, Dec. 2010.

[4] S. M. Asif, *et al.*, "Design and in vivo test of a batteryless and fully wireless implantable asynchronous pacing system," *IEEE Trans. Biomed. Eng.,* vol. 63, no. 5, pp. 1070-1081, May 2016.

[5] T. Campi, *et al.*, "Wireless power transfer charging system for AIMDs and pacemakers," *IEEE Trans. Microw. Theory Techn.,* vol. 64, no. 2, pp. 633-642, Feb 2016.

[6] S. M. Asif, *et al.*, "A Novel RF-Powered Wireless Pacing via a Rectenna-Based Pacemaker and a Wearable Transmit-Antenna Array," IEEE Access, vol. 7, pp. 1139-1148, 2019.

[7] T. Campi, *et al.*, "Induced effects in a pacemaker equipped with a wireless power transfer charging system," *2016 IEEE Conf. Electromagnetic Field Computation (CEFC)*, Miami, FL, USA, 2016.

[8] M. Miller, *et al.*, "Leadless cardiac pacemakers- back to the future," *J. Amer. Col. Card.,* vol. 66, no. 10, pp. 1179-1189, Sep. 2015.

[9] Carnegie School of Engineering. [Online]. Available: https://www.engineering.cmu.edu [Last accessed: 10 September 2018].

[10] A. Haeberlin, *et al.*, "The first battery less solar powerd cardiaz pacemaker," *Heart Rhythm,* vol. 12, no. 6, pp. 1317-1323, 2015.

[11] S. M. Asif, *et al.*, "Computation of available RF power inside the body and path loss using in vivo experiments," IET Microw., Antennas & Propag., vol. 13, no. 1, pp. 122-126, January 2019.

[12] J. Olivo, *et al.*, "Energy harvesting and remote powering for implantable biosensors," *IEEE Sensors J.,* vol. 11, no. 7, pp. 1573-1586, July 2011.

[13] Medtronic Inc., MN, USA. [Online]. Available: http://www.medtronic.com [Last accessed: 10 September 2018].

[14] St. Jude Medical Inc., MN, USA. [Online]. Available: http://sjm.com/leadlesspacing [Last accessed: 10 September 2018].

[15] D. Ewert et al., "Intelligent self-organizing electrode stimulation delivery system," U.S. Patent 8,977,358, Oct. 2014.

[16] A. Kiourti and K. Nikita, "A review of implantable patch antennas for biomedical telemetry: Challenges and solutions," *IEEE Antennas Propag. Mag.,* vol. 54, no. 3, pp. 210-228, Jun. 2012.

[17] J. Kim and Y. Rahmat-Samii, "Implanted antennas inside a human body: simulations, designs, and characterizations," *IEEE Trans. Microw. Theory Techn.,* vol. 52, no. 8, pp. 1934-1943, Aug. 2004.

[18] K. S. Nikita, 2nd Ed., *Handbook of Biomedical Telemetry*. Wiley, 2014.

[19] Tissue Simulating Liquids. [Online]. Available: https://www.speag.com/products/ [Last accessed: 10 September 2018].

[20] A. Kiourti and K. S. Nikita, "A review of in body biotelemetry devices Implantables, ingestibles, and injectables," *IEEE Trans. Biomed. Eng.*, vol. 64, no. 99, pp. 1422-1430, 2017.

[21] R. A. Bercich, *et al.*, "Far-field RF powering of implanatable devices: Safety considerations," *IEEE Trans. Biomed. Eng.*, vol. 60, no. 8, pp. 2107-2112, 2013.

[22] J. W. Hansen, *et al.*, "A far-field radio-frequency experimental exposure system with unrestricted mice," *SpringerPlus,* vol. 4, pp. 1-13, Nov. 2015.

[23] L. Marnat, *et al.,* "On-chip implantable antennas for wireless power and data transfer in a glaucoma-monitoring SOC," *IEEE Antennas Wireless Propag. Lett.*, vol. 11, pp. 1671-1674, 2012.

[24] F. J. Huang, *et al.*, "Rectenna application of miniaturized implantable antenna design for triple-band biotelemetry communication," *IEEE Trans. Antennas Propag.*, vol. 59, no. 7, pp. 2646-2653, July 2011.

[25] S. Hu, *et al.*, "A low-cost 2.45-GHz wireless power link for biomedical devices," *IEEE Asia-pacific Conf. Antennas Propag.*, Singapore, pp. 215-216, August2012.

[26] A. Poon, *et al.*, "Optimal frequency for wireless power transmission into dispersive tissue," *IEEE Trans. Antennas Propag.,* vol. 58, no. 5, pp. 173-1750, 2010.

[27] A. Moglia, *et al.*, "Recent patents on wireless capsule endoscopy," *Recent Patents on Biomed. Eng.,* vol. 1, no. 1, pp. 24-33, 2008.

[28] J. Hao, *et al.*, "Wireless power transfer to deep-tissue microimplants," *PNAS*, vol. 111, no. 22, pp. 7974-7979, 2014.

[29] A. Kiourti, *et al.*, "A wireless fully passive neural recording device for unobtrusive neuropotential monitoring," *IEEE Trans. Biomed. Eng.,* vol. 63, no. 1, pp. 131-137, 2016.

[30] X. Li, "Body matched antennas for microwave medical applications," Ph.D. dissertation, Karlsruhe Institute of Technology, 2014.

[31] K. R. Foster and H. P. Schwan, "Dielectric properties of tissues and biological materials: a critical review," *Critical Rev. Biomed. Eng.,* vol. 17, no. 1, pp. 25-104, 1989.

[32] P. S. Hall and Y. Hao, "Electromagnetic Properties and Modeling of the Human Body", *Antenna and Propagation For Body-Centric Wireless Communications,* 2nd ed. , Artech House, pp. 11-34, 2006.

[33] ANSYS HFSS. [Online] Available: http://www.ansys.com [Last accessed: 10 September 2018].

[34] CST MICROWAVE STUDIO. [Online]. Available: https://www.cst.com [Last accessed: 10 September 2018].

[35] Sim4Life by SPEAG. [Online]. Available: https://www.zurichmedtech.com/ [Last accessed: 10 September 2018].

[36] P. Soontornpipit, *et al.*, "Design of implantable microstrip antenna for communication with medical implants," *IEEE Trans. Microw. Theory Techn.,* vol. 52, no. 8, pp. 1944-1951, 2004.

[37] T. Karacolak, *et. al.*, "Design of a dual-band implantable antenna and development of skin mimicking gels for continuous glucose monitoring," *IEEE Trans. Microw. Theory Techn.,* vol. 56, no. 4, pp. 1001-1008, April 2008.

[38] Z. Noroozi and H. F. Kashani, "Three-dimentional FDTD analysis of the dual-band implantable antenna for continuous glucose monitoring," in *Progress Electromag. Research Lett.,* vol. 28, pp. 9-21, April 2012.

[39] C. Gabriel, "Compilation of the Dielectric Properties of Body Tissues at RF and Microwave Frequencies" Brooks Air Force, TX, USA.: Tech. Rep. Report N.AL/OE-TR-. 31-CB, 1996.

[40] F. A. Duck, *Physical Properties of Tissues: A comprehensive Reference Book*, Elsevier Ltd., 1990.

[41] A. T. Mobashsher and A. M. Abbosh, "Artificial Human Phantoms," *IEEE Microw. Mag.,* vol. 16, no. 6, pp. 42-62, July 2016.

[42] M. Lazebnik, *et al.*, "Tissue-mimicking phantom materials for narrowband and ultrawideband microwave applications," *Phys. Med. Biology*, vol. 50, no. 18, pp. 4245-4258, 2005.

[43] J. Garrett and E. Fear, "Stable and felxible materials to mimic the dielectric properties of human sift tissues," *IEEE Antennas Wireless Propag. Lett.,* vol. 13, pp. 599-602, 2014.

[44] A. W. Guy, "Analyses of electromagnetic fields induced in biological tissues by thermographic studies on equivalent phantom models," *IEEE Trans Microw. Theory Techn.,* vol. 19, no. 2, pp. 205-214, February 1971.

[45] N. Chahat, *et al.*, "New method for determining dielectric properties of skin and phantoms at millimeter waves based on heating kinetics," *IEEE Trans. Microw. Theory Techn.,* vol. 60, no. 3, pp. 827-832, March 2012.

[46] A. T. Mobashsher and A. M. Abbosh, "Three-dimensional human head phantom with realistic electrical properties and anatomy," *IEEE Antennas Wireless Propag. Lett.,* vol. 13, pp. 1401-1404, 2014.

[47] Y. Nikawa, *et al.*, "Soft and dry phantom modeling material using silicone rubber with carbon fiber," *IEEE Trans. Microw. Theory Techn.,* vol. 44, no. 10, pp. 1949-1953, 1996.

[48] J. T. Chang, *et. al.*, "A conductive plastic for simulating biological tissue at microwave frequencies," *IEEE Trans. Electromag. Compat.,* vol. 42, no. 1, pp. 76-81, 2000.

[49] SPEAG, Human Body Tissue Simulating Liquids. [Online] Available: http://www.speag.com/products/dasy6/tissue-simulating-liquids [Last accessed: 10 September 2018].

[50] SPEAG, Dielectric Probe Kit. [Online]. Available: http://www.speag.com/products/dak/dielectric-measurements/ [Last accessed: 10 September 2018].

[51] W. L. Stutzman and G. A. Thiele, Antenna Theory and Design, 3rd ed. New York: Wiley, 2012.

[52] C. A. Balanis, Antenna Theory Analysis and Design, 4th ed. New York: Wiley, 2016. 51

[53] J. D. Baena *et. al.*, "Equivalent-circuit models for split-ring resonators and complementary split-ring resonators coupled to planar transmission lines," *IEEE Trans. Microw. Theory Techn.* vol. 53, no. 4, pp. 1451-1461, April 2005.

Sajid M. Asif (S'11-M'17) received the B.S. degree in electrical engineering (communication) from the University of Engineering and Technology, Taxila, Pakistan, in 2004, and the M.S. degree in radio frequency communication engineering from the University of Bradford, Bradford, U.K., in 2006. He received his Ph.D. degree in Electrical and Computer Engineering from North Dakota State University, Fargo, ND, USA in 2017. Prior to his Ph.D. degree, he was a Faculty Member in COMSATS University, Pakistan. Currently, he is a Research Associate in Frequency Agile Radio at the University of Sheffield, UK. He has authored and co-authored more than 50 journal and conference papers. His research interests include RF/microwave circuits, printed antennas, implantable antennas, wireless sensors, and energy harvesting for biomedical applications.

Dr. Asif was the Chair of the IEEE Red River Valley section from 2015 to 2016 and Vice Chair from 2014 to 2015. He has received numerous awards and scholarships, among which are the IEEE-AP-S Doctoral Research Award (2015) and the NSF funded ND-EPSCOR Doctoral Dissertation Assistantship Award for 2015-2016. He received the IEEE Outstanding Student Award (2016), won (first place) in the 2017 NDSU Innovation Challenge Competition (product category) and received the College of Engineering Graduate Researcher of the Year award in 2017. He is a member of IEEE, Tau Beta Pi, Golden Key International, and IEEE-Eta Kappa Nu.

Adnan Iftikhar (M'16) received his B.S. degree in electrical engineering from COMSATS University Islamabad (CUI), Pakistan, M.S. degree in Personal Mobile and Satellite Communication from University of Bradford U.K, and PhD. degree in Electrical and Computer Engineering from North Dakota State University (NDSU), USA in 2008, 2010, and 2016, respectively. Currently, he is an Assistant Professor in Electrical Engineering Department at CUI. He has authored and co-authored more than 30 peer-reviewed journal and conference publications. His main research domains include applied electromagnetics, reconfigurable antennas, and energy harvesting for low power devices. He is a member of IEEE.

Benjamin D. Braaten (S'02-M'09-SM'14) received the B.S. degree in electrical engineering in 2002, the M.S. degree in electrical engineering in 2005, and the Ph.D. degree in electrical and computer engineering in 2009, all from the North Dakota State University, Fargo, ND, USA. During the 2009 Fall semester, he held a Postdoctoral Research Position in the South Dakota School of Mines and Technology, Rapid City, SD, USA. At the end of the 2009 Fall Semester, he joined the Faculty of the Electrical and Computer Engineering Department, North Dakota State University, and was promoted to Associate Professor with tenure in 2015. He is the current Chair of the same department and has authored or co-authored more than 100 peer-reviewed journal and conference publications, several book chapters on the design of antennas for radio frequency identification, and holds one U.S. patent on wireless pacing of the human heart. His research interests include printed antennas, conformal self-adapting antennas, microwave devices, topics in EMC, topics in BIOEM, and methods in computational electromagnetics.

Dr. Braaten received the College of Engineering and Architecture Graduate Researcher of the Year and College of Engineering and Architecture Graduate Teacher of the Year awards. He also serves as an Associate Editor for the IEEE ANTENNAS AND WIRELESS PROPAGATION LETTERS and is a member of the IEEE, IEEE-Eta Kappa Nu, and National Honorary Mathematical Society PI MU EPSILON.

Daniel L. Ewert received the Ph.D. degree in physiology from the University of North Dakota, Fargo, ND, USA, in 1989. Since 1990, he has been a Professor of electrical and computer engineering at North Dakota State University, Fargo, ND, USA. He was also the Chair of the same department from 2001 to 2009. From 2010 to 2011, he was the Director of Iron Range Engineering program at Minnesota State University, Mankato, MN, USA. From 1989 to 1990, he held a Postdoctoral Research position at Mayo Clinic. He has performed cardiovascular engineering research with the US Air Force, NASA, Russian Space Agency, Birmingham Children's Hospital, England, and University of Louisville. He is the Founder and CEO of Krisara Engineering; a medical device start-up company. Currently, he is an Emeritus Professor at NDSU and Chief Innovation Officer at Anderson Industries-IronMaster Innovation Center, Mapleton, ND. His research interests include cardiovascular engineering and wireless biomedical sensors.

Keith Maile (BSEE 1986, MSEE 1990, PhD 1993) is an expert in assessing technologies, architecting electronics, selecting/designing physiological and physical sensors for both implantable and wearable medical devices, wireless power transfer and powering methods and analog low-power CMOS circuit design for implantable medical applications. He is a driven individual with very analytical skills. In his 32 years of experience, he has been employed by three companies (Honeywell:1986-1989, Boston Scientific-formerly Guidant:1989-2000, 2002-present and Applied Micro Circuits Corp: 2000-2002). Most of his tenure was spent at CPI/Guidant/Boston Scientific where he worked on both platform-designs for near-term products (which provided the main revenue stream) as well as product and/or feature concepts. In these roles, he performed as a technical leader of teams for the hardware development as well as performing as an individual contributor in analog circuit design and sensor design for both physical and physiologic needs. As of late, his role has shifted to technical strategy where performs exploratory and white-space research in the areas of sensors and other technologies that should be considered for future products. He spent 2 years at AMCC focusing on the development of analog high-speed bipolar IC's for 10 and 40Gb/s fiber-optic communication systems. This work included the development of integrated high-speed circuits, transmission lines and distributed networks. At Honeywell, he worked on analog circuits for the signal conditioning of base-band MMW-radar.

Dr. Maile is currently a Senior Fellow Engineer in the Rhythm Management group for Boston Scientific Inc. in Arden Hills, Minnesota, USA. He currently has roughly 70 issued patents and more than 30 applied for.